SHM of Single Lap Adhesive Joints using Subharmonic Frequencies

D. Ginzburg [a], F. Ciampa [a], G. Scarselli [b], M. Meo *[a]

[a] Material Research Centre, Department of Mechanical Engineering,
University of Bath, Bath, BA2 7AY, UK
[b] Department of Engineering for Innovation, University of Salento,
Via per Monteroni (Lecce), 73100, Italy

* Corresponding author: m.meo@bath.ac.uk

Abstract

The increased usage of adhesive bonding as a joining method in modern aerospace components has led to developing reliable ultrasonic health monitoring systems for detection of regions of poor adhesion. Nonlinear acousto-ultrasonic techniques based on higher harmonics and subharmonic frequencies have shown to be sensitive to the detection of micro-voids and disbonds. Nonlinear resonance properties of disbonds generate various nonlinear phenomena such as self-modulation, subharmonics, hysteresis and so on. By exploiting the local natures of these phenomena, this paper demonstrates the use of subharmonics for detection and imaging of flaws in bonded structures. Due to the lack of both analytical and numerical models able to optimise the experimental testing, this paper also proposes a two-dimensional analytical model and a three-dimensional finite element analysis (FEA) simulation for the generation of nonlinear elastic effects with emphasis on subharmonic frequency components The proposed analytical model qualitatively described the generation of subharmonics but also higher harmonics due to the nonlinear intermodulation of the driving and resonance frequencies associated with the disbonded region. The numerical model was developed by modifying the user defined cohesive element formulation with a quadratic traction-displacement relationship in order to simulate the interaction of elastic waves with the structural disbond. Whilst the analytical model supported the selection of the driving frequency, the numerical one successfully predicted the generation of subharmonic frequencies originating in the disbonded area. Experimental tests were conducted on a disbonded single lap joint structure using surface-bonded piezoelectric transducers and a laser-Doppler vibrometer (LDV), and allowed to validate the analytical and numerical results. It was clearly demonstrated that the nonlinear resonance effects in the form of subharmonics could be used to discriminate reliably regions of poor adhesion in bonded structures. This work can lead to new in-situ nonlinear acoustic based health monitoring system for locating and imaging defects in critical aerospace components.

Keywords: single lap joints, nonlinear local defect resonance (LDR), subharmonic resonance, SHM

Introduction

There are a number of structural applications where the only feasible method of joining components together is by means of an adhesive. This approach presents several advantages in terms of cost and ease of manufacturing, light weight, optimum stress distribution in the bonded region, and the ability to join dissimilar materials. While the in-service behaviour of the mechanical fasteners (e.g. rivets, bolts, screws etc.) and welds has been well understood, the same cannot be said about the adhesive joints. Partial disbonds and voids are typical defect types characteristic to the bonded structures. In the past several decades, a considerable research effort has been focused on investigating their effects on the bond strength, the dynamic response of the adhesive joints and the development of the appropriate non-destructive evaluation (NDE) techniques for detection, localisation and sizing of the bond related defects. Indeed, with growing design complexities, reliable NDE methods are required for disbond detection and evaluation in situations when a direct physical access to a component for inspection may not be possible (e.g. internal structure of an aircraft wing). Traditional linear acousto-ultrasonic testing NDE inspection techniques typically involve detecting the reflection and scattering of primary waves at material discontinuities [1] with subsequent imaging of signal amplitude and phase. As the frequency response of a structure changes in the presence of disbonds/voids [2], acoustic emission (AE) and the level of damping can also be used as a measure of bond strength [3, 4]. Among linear ultrasonic methods, the Electromechanical Impedance (EMI) technique has provided valuable insight on the inspection of single lap joints by using both undamaged and disbonded coupons [5], [6]. A disbond present in a structure is generally termed in literature as a kissing bond, which is characterised by the two compressed but otherwise unbounded surfaces [7]. The resulting change in stiffness and acoustic impedance in the vicinity of kissing bonds is typically very small and therefore little or no energy is reflected for the detection using the standard linear pulse-echo approach [8]. Therefore, the effectiveness of the linear techniques is limited in cases when a crack or disbond is fully/partially closed due to a closure stress or oxide films [9].

A number of authors [10, 11] have experimentally shown that defects such as kissing bonds characteristic to adhesive joints can be detected using alternative acousto-ultrasonic techniques known as nonlinear elastic wave spectroscopy (NEWS) methods [12-15] that rely on detection of acoustic nonlinearities arising from discontinuities and defect-related hysteresis in the media. Hysteretic nonlinearity, which is characterised by a strongly nonlinear hysteretic stress-strain relation, occurs in heterogeneous materials containing inclusions such as cracks, grain contacts and dislocations at micro and mesoscopic level [16]. At the basis of these nonlinear methods is the hypothesis that at the sufficient amplitude of excitation, the wave propagating through a region containing a defect will cause the medium to respond in a nonlinear fashion. In a classical view of nonlinear ultrasonics, the nonlinearities arise due to local velocity variations which in turn cause the waveform to deform and transition from a harmonic wave into a saw-tooth type one as it propagates through a nonlinear medium [16]. As the result, a wave of an amplitude Q_0 and frequency f_0 propagating through the defects such as kissing bond will contain multiples (harmonics) of the driving frequency (f_0), namely $2f_0$, $3f_0$, etc. with the corresponding amplitudes Q_1, Q_2, etc.; harmonic frequencies above the f_0 are termed higher harmonics or super-/ultra- harmonics, while the ones below f_0 are denoted subharmonics. Subsequently, the extent of the defect can be evaluated by measuring the level of these nonlinearities. In the kissing bond region, the mechanism of the harmonics generation is hypothesized to be driven by the opening and closing of the contact interface as the wave travels. This phenomenon is sometimes referred to as “clapping”, and “rubbing” and is more broadly defined as contact acoustic nonlinearity (CAN) by [9, 16-18]. The interface between the fractured or debonded

surfaces can exhibit some degree of altered residual normal and shear stiffness in compression and/or tension due to the presence of contaminants or surface roughness. The “clapping” behaviour can be described using a quadratic stiffness response considering perfectly flat surfaces [19].

Utility of the second order harmonic amplitude for damage characterisation of materials is principally associated with the media that manifest classical nonlinear behaviour [20] at the atomic/molecular scale. While classical and non-classical NEWS methods were demonstrated to be effective in certain conditions, it is important to note that many materials including the substrate (e.g. aluminium or composite plates) and the adhesive itself can exhibit the aforementioned nonlinear behaviour even in a defect free state. Indeed, it is well known that a wave propagating through a fluid such as water attains second and higher order harmonics. Moreover, the signal-to-noise ratio (S/N) of defect generated harmonics is typically very low as the equipment (e.g. waveform generators, amplifiers, transducers etc.) also produce these nonlinear effects [9]. This leads to an essential requirement for any NDE method based on the nonlinearity measurement to be capable of reliably discerning between the inherent system nonlinearity (e.g. due to instrumentation) and the defect related one (e.g. CAN).

In addition to the classical nonlinear effects, several “non-classical” nonlinear wave phenomena such as local defect resonance (LDR) effects were experimentally observed and investigated [21, 22]. In essence, the LDR is conceptually based on the premise that inclusion of a defect in a material results in a local rigidity decrease of a certain mass associated with the defect area which in turn should lead to the manifestation of a specific frequency, characteristic of the defect [22]. Unlike the resonance of the whole specimen, an efficient generation of harmonics and wave mixing can be achieved even at moderate input signal levels by exciting a specimen at the LDR frequency associated with the defect [22]. A successful application of this technique requires a definitive identification (analytically, numerically or experimentally) of the defect resonance frequency, which can be analytically estimated for certain artificial defect types such as flat bottom holes (FBH) [23]. Furthermore, LDR effects can generally be classed as linear and nonlinear with the former simply referring to an increase in amplitude of vibration in the vicinity of the defect. In the nonlinear case, the LDR generally corresponds to an interaction of acousto-ultrasonic waves with the damage/defect at a frequency matching the defect resonance, which in turn tends to result in a considerable amplification of local vibration amplitude in the damage region. Several recent studies showed the application of the phenomenon of linear and nonlinear LDR in non-contact NDE techniques for the detection of artificial defects in metals and composite materials using digital shearography [24], and in detection of impact-induced delamination in CFRP and GFRP composite materials using the laser-Doppler vibrometer (LDV) imaging [22]. Furthermore, amplitude-dependent dynamic resonance frequency shift occurring locally to the defect area can be used as an indication of the severity of the damage [22]. In terms of LDR, this effect occurs locally to the defect, which contrasts the nonlinear ultrasonic spectroscopy (NRUS) [25] in the sense that NRUS works on the principle that the resonance frequency of the whole structure shifts as the strength of the nonlinearity increases in a damaged material. However, the locality of LDR is an advantage as well as a detriment. Although, the concept of LDR showed promising results in some non-contact NDE applications, where the detector in the form of digital camera or LDV focused exclusively on the damage area, the use of LDR in contact applications (e.g. using piezoelectric transducers) is still limited. This implies that the LDR-enhanced nonlinear damage response can be sensed merely at the defect location.

Several studies focused on the generation and nonlinear imaging of the subharmonic frequency components in the response spectrum [9, 26, 27]. NEWS techniques based on the subharmonic sensing are advantageous as the resulting spectrum is virtually unhindered by the intrinsic presence of the classical nonlinear effects and instrumentation harmonics. However, certain conditions in terms

of the excitation configuration must be met for the subharmonic frequencies to manifest in such a way that allows qualitative and/or quantitative evaluation of the defects at the macroscopic (structural) level. Johnson et al. devised a single degree of freedom crack model based on the dual stiffness oscillator which indicated that production of subharmonics appreciably increased close to twice the natural frequency of vibration. Wang et al. [26] numerically and experimentally confirmed this behaviour using a metallic structure with a fatigue crack by applying the excitation frequency twice the value of the natural mode of the structure; the one dimensional numerical crack model was based on a linear oscillator with a hysteretic crack-related force formulation originally proposed by Delrue and Van Den Abeele [28]. An analytical basis for the generation of the subharmonic frequencies in one dimensional space was provided by Solodov et al. [27], while a two dimensional numerical finite difference model was proposed by Yamanaka et al. [29], whose crack model incorporated adhesion and atomic related stresses.

In present study, an analytical description of nonlinear elastic effects with emphasis on subharmonic generation associated with fully contact nonlinear LDR is provided considering a plate in pure bending subjected to a harmonic point load. The analytical model qualitatively indicated the generation of higher harmonics and the combination frequencies corresponding to the nonlinear intermodulation of the driving and the LDR frequencies, namely f_0 and f_d respectively. Subsequently, a single lap joint (SLJ) structure comprised of two isotropic plates partially joined with an adhesive was considered in the experimental and numerical campaign. The aim was to identify f_d of the debonded region and use the subharmonic component of the combination frequencies to perform nonlinear sensing and imaging of the defect. The numerical modelling was performed by means of commercial finite element analysis (FEA) software LS-DYNA® incorporating user defined cohesive elements representing the disbond, while an experimental validation utilised piezoelectric transducers and LDV.

2–D Analytical Model for Nonlinear LDR Subharmonic Generation

As mentioned earlier, the LDR can increase the amplitude and the detectability of classical nonlinear response (e.g. higher harmonic generation and wave mixing) of the defects via local vibration amplification even at moderate levels of input signal. However, there are other dynamic nonlinear phenomena that are characteristic to resonant defects which include nonlinear resonance, subharmonics generation [26, 27], parametric (amplitude-dependent) resonance [20] and self-modulation [27]. To analytically demonstrate the existence of these effects and their respective spectral components, it is assumed that the damaged region manifests both resonance and nonlinear properties and therefore can be defined as an anharmonic (nonlinear) oscillator. Following the formulation and notation of Landau and Lifshitz [20], the equation of motion for an nonlinear oscillator in one dimension can be stated as

$$\ddot{x} + \omega_0^2 x = \frac{Q_0}{m} \cos f_0 t - \xi x^2, \tag{1}$$

where x is displacement, Q_0 and f_0 are the amplitude and frequency of the excitation force, m is the structural mass; ω_0 is the resonant angular frequency of the system in absence of friction (damping), driving forces and the nonlinear term; ξx^2 is the second order nonlinear term of the anharmonic oscillator with its respective coefficient (constant) ξ. Assuming the driving force is reasonably small and the nonlinear terms are much smaller than the linear one, a well-known perturbation method can be used by seeking a solution to Eq. (1) in a form of a series of successive approximations

$$x = x^{(1)} + x^{(2)}, \tag{2}$$

where $x^{(1)} = A(f_0)\cos f_0 t$ is a harmonic function of amplitude A representing a solution to the linear case in absence of damping, the driving force and the nonlinear terms, and $x^{(2)}$ represents the solution of the second order nonlinear term ξx^2. Setting $f_0 = 2\omega_0 + \varepsilon$ with small ε (i.e. driving frequency near double the resonant value), Eq. (1) can be solved resulting in a condition for subharmonic resonance with the solution comprising subharmonic frequency outputs $\omega = f_0/n$ (*n*= 2, 3, …) [20, 30].

Following the formulation for an anharmonic oscillator expressed by Eq. (1) in the absence of in-plane and thermal forces and excluding effects of damping, a 2-D nonlinear equation of motion governing the bending of thin (span-to-thickness ratio greater than 10) homogeneous isotropic plates of length *a* and width *b* subjected to a sinusoidal transverse force q can be stated as follows

$$D\left(\frac{\partial^4 w_0(x,y,t)}{\partial x^4} + 2\frac{\partial^4 w_0(x,y,t)}{\partial x^2 \partial y^2} + \frac{\partial^4 w_0(x,y,t)}{\partial y^4}\right) + I_0 \frac{\partial^2 w_0(x,y,t)}{\partial t^2} + \\ - q(x,y,t) + q^{NL}(\xi,x,y,t) = 0, \tag{3}$$

where D is the bending/flexural rigidity of the plate, w_0 is the transverse (out-of-plane) displacement which is a function of (x, y) coordinates and the time variable t, I_0 is the mass moment of inertia,

q^{NL} is a nonlinear force term which can be a sum of quadratic and cubic terms as in Eq. (2) , although, only the second order one (q^{II}) was considered in this study

$$q^{NL}(\xi,x,y,t)=q^{II}(\xi,x,y,t), \tag{4}$$

where ξ is the second order nonlinear coefficient (constant). Assuming that $q^{NL} << q$ and setting the boundary conditions of a simply supported plate at all four edges and initial conditions such that $w_0(x,y,0)=0$ and $\partial w_0(x,y,0)/\partial t=0$ are zero, a first order perturbation theory can be used to solve Eq. (3) in the form

$$w_0(x,y,t)=w_0^{(1)}(x,y,t)+\xi w_0^{(2)}(x,y,t). \tag{5}$$

Assuming a harmonic input $Q_0\cos(2\pi f_0 t)$ as a point source at (x_0,y_0) having an amplitude Q_0 and the driving frequency f_0 , the solution of the linear inhomogeneous problem can be obtained via series expansion of the transverse deflection $w_0^{(1)}(x,y,t)$ and load $q(x,y,t)$ for $t\geq 0$ as follows [31]

$$w_0^{(1)}(x,y,t)=\sum_{n=1}^{\infty}\sum_{m=1}^{\infty}A^I L_1\sin(\alpha x)\sin(\beta y), \tag{6}$$

where $L_1=\cos(2\pi f_0 t)-\cos(2\pi f_{mn}t)$, $A^I=Q_0/\pi^2 abI_0\left(f_{mn}^2-f_0^2\right)$, $\alpha=m\pi/a$, $\beta=n\pi/b$ and f_{mn} is a series of resonant frequencies for simply supported plate with $m,n=1,2,3,\ldots$. The particular linear solution corresponds to the steady state oscillation of the plate at the frequency f_0 of the excitation force. Similarly, taking f_d as the LDR frequency associated with the defect at the location (x_d,y_d) and assuming an expansion of the nonlinear out-of-plane displacements and transverse loads, the second order ($w_0^{(2)}$)nonlinear solutions can be obtained in the form shown by Eq. (7)

$$w_0^{(2)}(x,y,t)=\sum_{n=1}^{\infty}\sum_{m=1}^{\infty}\left[\frac{\overline{A}^{II}}{2}(S_1+S_2+S_3+S_4)\right]\sin(\alpha x)\sin(\beta y), \tag{7}$$

where $A^{II}=\left[Q_0\sin(\alpha x_d)\sin(\beta y_d)/\pi^2 abI_0\left(f_d^2-f_0^2\right)\right]^2$ with $\overline{A}^{II}=A^{II}/I_0$.

S terms in Eq. (7) correspond to a number of nonlinear elastic phenomena associated with the local resonance at the defect location and can be defined as follows

$$S_1=\frac{[1-\cos(2\pi f_{mn}t)]}{2\pi^2 f_{mn}^2}, \tag{8}$$

$$S_2=\frac{\cos(2\pi f_{mn}t)-\cos(4\pi f_0 t)}{4\pi^2\left(4f_0^2-f_{mn}^2\right)}, \tag{9}$$

$$S_3=\frac{\cos(2\pi f_{mn}t)-\cos(4\pi f_d t)}{4\pi^2\left(4f_d^2-f_{mn}^2\right)}, \tag{10}$$

$$S_4=\frac{2[\cos[2\pi(f_0\pm f_d)t]-\cos(2\pi f_{mn}t)]}{\left[(2\pi f_0\pm 2\pi f_d)^2-4\pi^2 f_{mn}^2\right]}, \tag{11}$$

Of particular interest to this work is the term S_4 (Eq. (11)) containing the combination frequencies $(f_0\pm f_d)$ which gives rise to the generation of subharmonic frequency (f_0-f_d) in case f_0 is chosen

such that f_0 =2 f_d . In other words, exciting a sample at double of LDR frequency corresponding to the disbond should lead to the generation of sidebands at $f_0 - f_d = 2f_d - f_d = f_d$. This term is of primary interest in this study as the subharmonic components in the spectrum are less susceptible to the instrumentation effects.

Experimental Setup and Procedure

The single lap joint (SLJ) samples were manufactured using two aluminium plates partially joined by the adhesive (Table 1). Prior to bonding, the joint surfaces were polished with emery paper and cleaned with acetone; the procedure advised by the manufacturer was followed for the application of the adhesive. The nominal thickness of the applied adhesive was 0.15 mm. Artificial defects in the form of disbonds (voids) were introduced by careful application of the adhesive and placing a Teflon sheet in the desired debonded region during the manufacturing process. Afterwards, the samples were inspected using an ultrasonic C-scan method in order to ensure that the samples conformed to the specification set for the debonded area. In the experimental setup, two piezoelectric (PZT) transducers were bonded to the surface of the samples in order to generate and receive the acousto-ultrasonic waves. During the testing, the samples were simply supported on two opposite edges by placing them on two blocks of acoustic foam. The dimensions and the material properties of the test samples are shown in Figure 1 and Table 1 respectively.

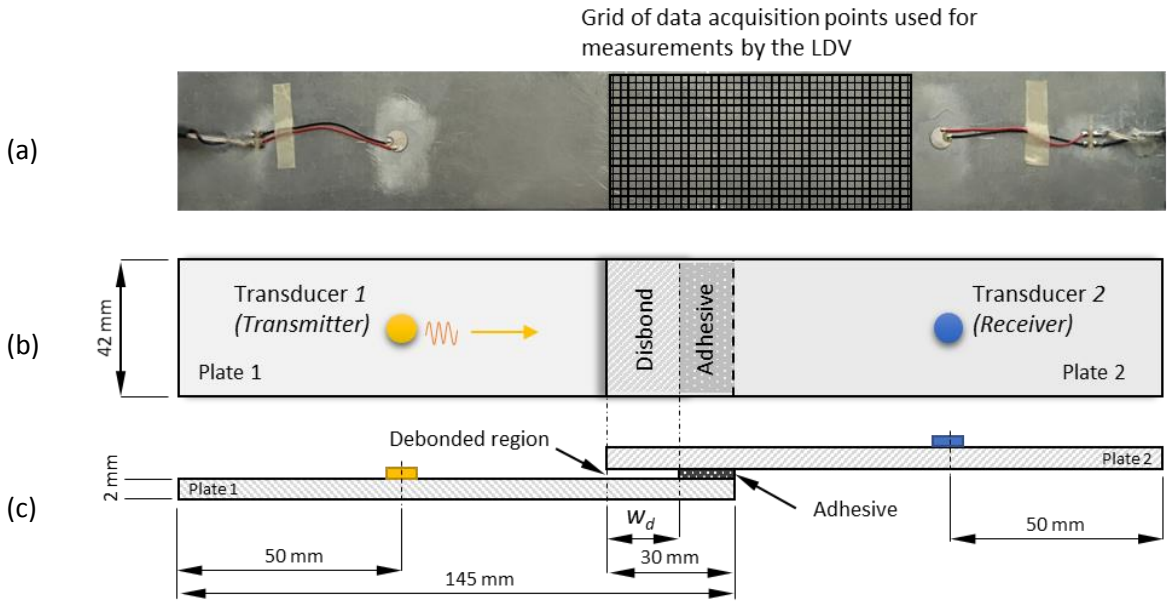

Figure 1: (a) a photograph of one of the actual SLJ samples with an overlaid grid of data points as used in the laser-Doppler vibrometer (LDV) experiments, (b) and (c) are the schematics of the top and side views with the specified dimensions.

	Young's modulus (GPa)	Mass density (g/cm^3)	Poisson's ratio
Aluminium (6061) plate	71	2.77	0.33
Araldite 2012A adhesive	1.654	1.17	0.3

Table 1: material properties.

The experimental campaign aimed at evaluating the presence of the disbond and its location by harmonically exciting the sample with piezoelectric (PZT) transducer 1 and analysing the spectral

response. A number of samples were manufactured with different widths (w_d) of debonded areas. The specifications of the samples is provided in Table 2.

No.	Number of samples	Recess (disbond) width w_d (mm)
1	3	0 (fully bonded)
2	3	10
3	3	20

Table 2: specification of the recess areas used in SLJ samples.

In the present methodology, two testing procedures were carried out. The first one (refer to Figure 2(a)) involved capturing the response at the receiving PZT (transducer 2) without the use of the laser-Doppler vibrometer (LDV). A single tone signal was sent within a duration period of 100 ms until a steady-state material response at each driving frequency was achieved. Such a procedure was employed in order to increase the repeatability of results for the generation of subharmonic frequencies. In particular, a range of frequencies in the range from 10 kHz to 40 kHz with an increment of 5 Hz were transmitted from PZT 1 and the response was captured with PZT 2. After waiting 100 ms, a continuous single tone sinusoidal wave of 3 seconds in duration and an amplitude of 50 Vpp (Volts peak-to-peak) was sent to PZT 1 and recorded five times at each frequency; subsequently, the corresponding averaged frequency spectrum was evaluated.

The choice of input voltage is crucial for the successful generation of subharmonics. As stated by several authors [32], the subharmonics tend to exhibit a "threshold behaviour" which is characterised by a substantial increase in amplitude of subharmonic spectrum component after a certain input amplitude is exceeded. The excitation amplitude of 50 V_{pp} used in this study, which is similar to the level reported in literature [22, 26], was set by gradually increasing the excitation amplitude until the subharmonic level becomes constant.

A programme was written in LabVIEW software that interfaced between the PC and the waveform generator which allowed to automate the process of sending and acquiring the signals. This process could have been performed using the LDV which operates based on the principles of Doppler-effect and sensing the frequency shift of back scattered light from a moving surface. However, due to the limitations of the LDV software, implementing the automation procedure proved challenging. Moreover, the testing procedure that involves the PZT transducers without the use of LDV is more affordable and practical solution in terms of real world applications as the LDV equipment is a high cost asset and requires a direct line of sight with a test component.

LDV setup as shown in Figure 2(b) was used to capture the vibration velocity of the surface of the specimens.

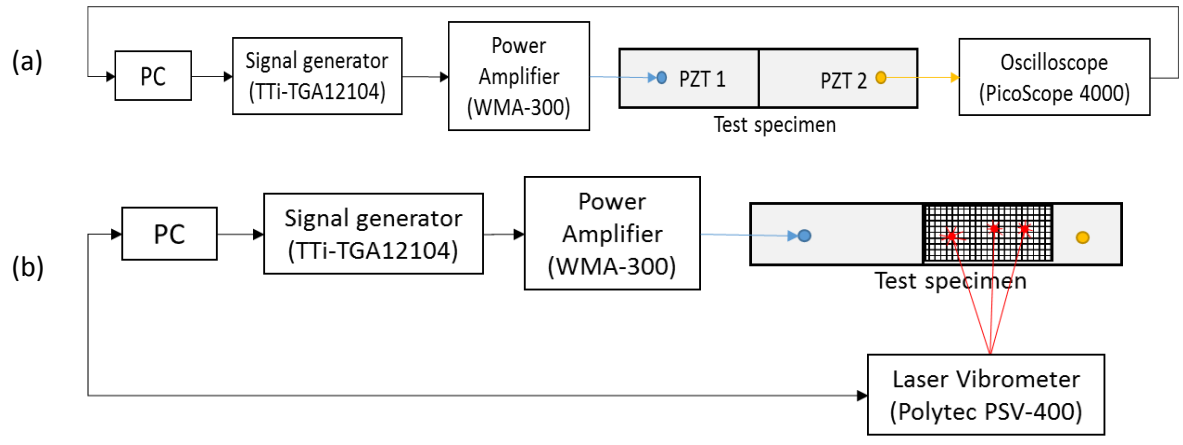

Figure 2: (a) test setup with piezoelectric transducers and (b) the LDV.

Numerical Model

In this study, a commercial FEA code LS-DYNA® was used to perform structural modal and dynamic analyses. In the modal analysis, the eigenvalues and their corresponding eigenfunctions were extracted which are associated with the natural frequencies and modes of free vibration of the structure. Hence, each possible resonance frequency with the corresponding vibration pattern can be plotted allowing an LDR frequency to be readily identified.
The dynamic part aimed at simulating a wave propagation phenomena mimicking the experimental setup presented earlier. Figure 3 presents a computational domain (finite element (FE) mesh) used for the analysis.

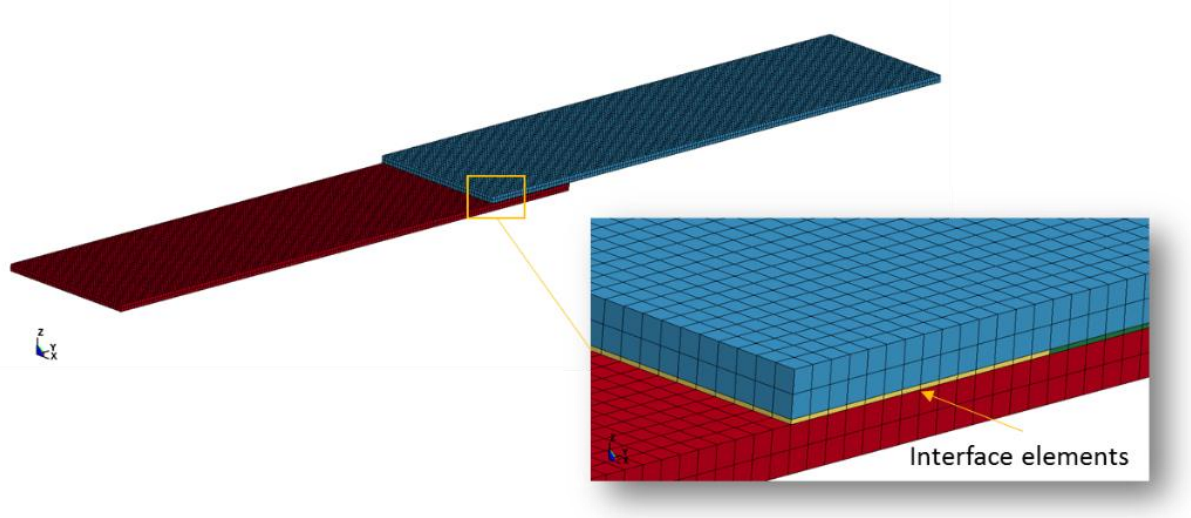

Figure 3: FE mesh.

Both the aluminium plates and the adhesive were modelled as isotropic elastic materials with the properties displayed in Table 1, whereas the disbond was modelled using a more special treatment.
While in the physical experiments, the dynamic interaction was allowed by contact between the upper and lower surfaces (i.e. kissing bond) of the plates in the overlapping area with no adhesive on (i.e. the debonded area), the interface (cohesive) elements represented this interaction in the numerical domain for the purpose of dynamic analysis. In the cohesive element formulation, the separation (relative displacement) between the upper and lower surface of the element is resisted by a nonlinear force-displacement relationship. Essentially, cohesive elements act as nonlinear springs connecting the opposing surfaces; instead of strains, the deformation is in terms of the relative displacements between the upper and lower surfaces of the element interpolated to the Gauss integration points; the force per unit area (traction) is used in the formulation. Cohesive zone models (CZM) are typically used for analysis of bonded structures such as composite panels where the crack path is known a priori and can be used to simulate a separation of the two adjacent layers (i.e. delamination). In this study, the cohesive element formulation with a quadratic traction-displacement relationship was implemented by means of a user defined cohesive material model interface of LS-DYNA in order to represent a nonlinear contact behaviour in the disbond. An alternative method could be to use one of the contact algorithms of LS-DYNA to simulate the interaction between the plates. However, no user defined capability currently exists for this purpose and all built-in contact algorithms are represented as linear springs.
In the cohesive element formulation, the tractions are calculated in the local coordinate system on the mid-surface defined half way between the upper and lower nodes (i.e. node pairs 1-5, 2-6, 3-7, 4-8 – refer to Figure 4).

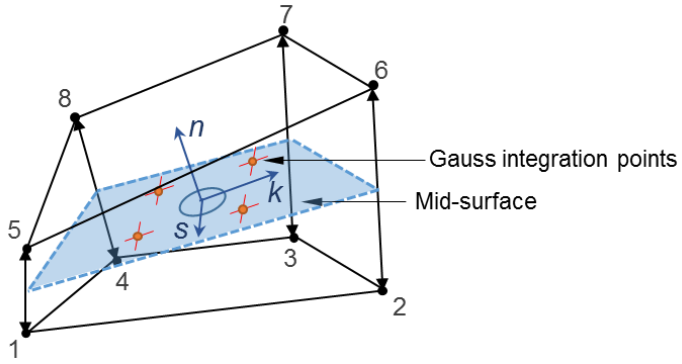

Figure 4: a schematic view of an 8-node cohesive finite element.

The relative displacements at an integration point at the of the element can be defined as follows

$$\Delta u = R^T \sum_{i=1}^{4} N_i(s,k)\Delta x_{i+4,i} - R_0^T \sum_{i=1}^{4} N_i(s,k)\Delta X_{i+4,i}, \quad \text{for i=1 to 4,} \tag{12}$$

where *s*, *k* and *n* denote the local coordinates, where components *s* and *k* are in-plane of the cohesive surface and *n* is normal to the plane; $\Delta x_{i+4,i}$ and $\Delta X_{i+4,i}$ are the coordinates in the current and the reference (initial) configurations respectively with subscripts referring the node pairs; R^T and R_0^T is a transpose of a rotation matrix from local to a global coordinate system in the current and the initial configuration respectively; N is a matrix of element shape functions which in the case of the present cohesive elements are linear interpolating functions used to calculate continuous fields (e.g. displacements) from discrete nodal displacements. Once the displacements are known, the tractions can be calculated as follows

$$\begin{Bmatrix} t_s^c \\ t_k^c \\ t_n^c \end{Bmatrix} = \begin{bmatrix} E_s & 0 & 0 \\ 0 & E_t & 0 \\ 0 & 0 & E_n \end{bmatrix} \begin{Bmatrix} \Delta u_s \\ \Delta u_k \\ \Delta u_n \end{Bmatrix}, \tag{13}$$

where t_s^c and t_t^c are in-plane tractions (N/mm^2), and t_n^c is normal traction (N/mm^2) – superscript is used to avoid confusion between the tractions associated with the cohesive and standard finite elements; E_s, E_t and E_n are the in-plane and the normal element stiffness (N/mm^3) respectively; Δu are the relative displacements (mm) at an integration point. The kissing bond was assumed to be dependent only on the normal stiffness [28, 33] (i.e. only "clapping" and no "rubbing" phenomena), and therefore, the shear components E_s and E_t were set to zero. Similarly to the reported mechanical diode crack models [34, 35], the following traction-displacement relationship was implemented

$$t_n^c = \begin{cases} 0 & \Delta u_n \geq 0 \\ E_{n1}\Delta u_n + E_{n2}\Delta u_n^2 & \Delta u_n < 0 \end{cases}, \tag{14}$$

where E_{n1} and E_{n2} were set to 5 x 10^3 (N/mm^3) and 3 x 10^3 (N/mm^3) respectively based on the coefficients reported by [28]. According to Eq. (14), there is zero stiffness when the plates are moving apart and nonlinear stiffness when the plates are moving closer together which is graphically represented in Figure 5 below.

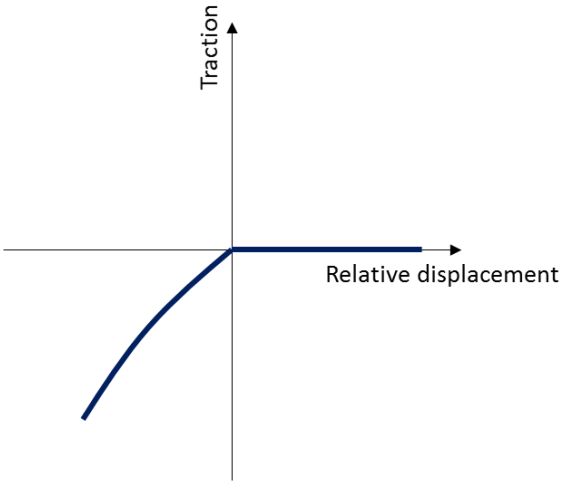

Figure 5: quadratic traction-displacement law used to represent the stiffness of the cohesive elements.

Subsequently, the nodal forces are obtained by integrating the tractions over the mid-surface of the cohesive element using 2 x 2 Gauss integration points and rotating them into the global coordinate system

$$\mathbf{F}^{coh} = \sum_{e=1}^{n_{el}} \mathbf{L}_e^T \left[\mathbf{R} \int_{\Gamma_e^c} \mathbf{t}^c \mathbf{N} d\Gamma \right], \tag{15}$$

where Γ_e^c is the boundary of the cohesive element; $\mathbf{t}^c$ is the vector of traction forces per unit area in the element coordinate system; $\mathbf{L}_e$ is the Boolean connectivity matrix which is used to collect the element forces into a global force matrix.

The governing equation can be written in a discreet form as follows

$$\mathbf{M\ddot{u}} = \mathbf{F}^{ext} - \mathbf{F}^{int} - \mathbf{F}^{coh}, \tag{16}$$

where $\ddot{\mathbf{u}}$ is the second time derivative of the global displacement vector, $\mathbf{F}^{ext}$ is the vector of externally applied forces and $\mathbf{F}^{int}$ is the global internal forces vector obtained by scattering each element vector into the global element array.

Equation (16) represent a system of nonlinear second order differential equations which are solved using explicit finite element code using direct time integration technique. Explicit time integration scheme of LS-DYNA was used as it is well suited for simulating wave propagation that lasts on the order of milliseconds. The global displacements at time $t + \Delta t$ using the central difference method is given by

$$\mathbf{u}_{t+\Delta t} = \Delta t^2 \mathbf{M}^{-1} \left(\mathbf{F}_t^{ext} - \mathbf{F}_t^{int} - \mathbf{F}_t^{coh} \right) - \mathbf{u}_{t-\Delta t} + 2\mathbf{u}_t, \tag{17}$$

where Δt is time increment or time step. Explicit time integration is computationally inexpensive for small durations and is conditionally stable – CFL (after Courant, Friedrichs and Lewy) stability criterion must be satisfied

$$\Delta t < \Delta t_{critical},$$

$$\Delta t_{critical} \leq \frac{2}{\omega_{max}}, \tag{18}$$

where ω_{max} is the highest natural frequency of the system, which for the assembled finite element model is bounded by the maximum frequency of the unassembled and unsupported elements. Physically, this means that Δt must be small enough that the information doeas not propagate across more than 1 element per time step. Therefore, a choice of element size for finite element mesh is very important. Material parameters and the size of finite elements directly affect the critical time step size. In present analysis, the maximum frequency of interest was of the order of 50 kHz which leads to a sampling rate of 2 Msps (megasamples per second) in case 40 points per wave length are desired. This information combined with the elastic properties of aluminium material yields an element size of 3.1mm for an 8-node fully integrated finite element. To achieve further increase in spectral resolution, an element size of 1 mm was used for the mesh of the aluminium plates. Free-free boundary conditions were used as it better represented the experimental setup. The loading was applied as harmonic force acting on the area of the nodes representative of the area of the PZT

$$F(t) = \bar{t}_z = Q_0 \sin(2\pi f_0 t), \tag{19}$$

where $\bar{t}_z$ is the force acting in the normal (z) direction which is prescribed on the nodes representing the PZT as shown in Figure 6; Q_0 is the excitation amplitude, f_0 is the fundamental frequency of the excitation and t is a time variable.

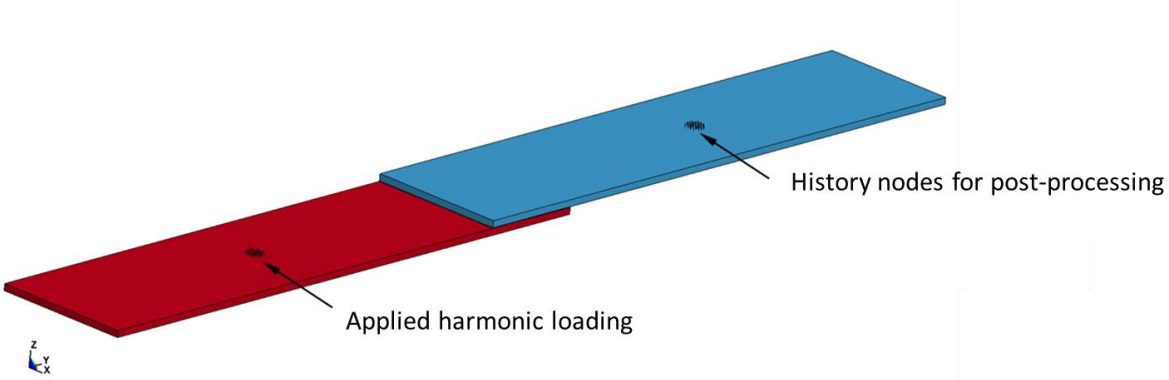

Figure 6: position of the loading and history nodes as used in the numerical analysis.

The out-of-plane displacement and velocity values were recorded during the simulation at the history nodes shown in Figure 6. The history data was averaged among these nodes in the post-processing step.

Results and Discussion

While an LDR frequency (f_d) can be analytically obtained for several types of internal defects by making certain assumptions about their geometry [23], no analytical expression yet exists so that the LDR can be readily calculated for an arbitrary defect type or a disbond featuring in the present study. By means of modal analysis [36, 37] using LS-DYNA, a natural frequency associated with the mode of vibration that displayed an apparent interaction in the debonded region was identified and used as f_d . The corresponding flexural modal shape of a sample with a recess (disbond) width w_d of 20 mm is shown in Figure 7. A flexural mode of vibration was chosen as previous research efforts indicated a possible correlation between the subharmonic generation and the flexural mode in an aluminium sample with a fatigue crack [26].

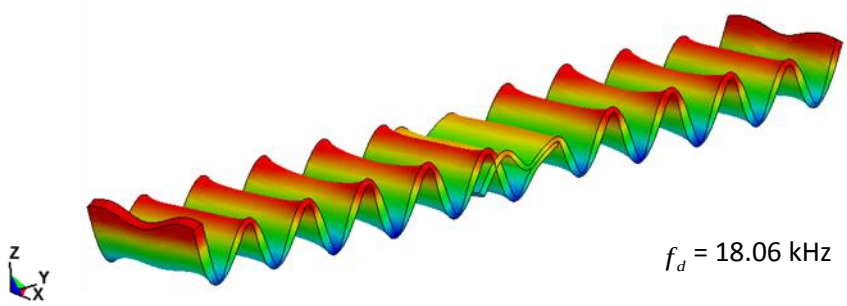

Figure 7: a flexural mode shape of vibration as predicted by modal FEA (LS-DYNA).

Guided by the LDR frequency (f_d) determined by the FEA, the first part of the experimental campaign aimed at identifying the frequency corresponding to the same mode of vibration in a physical sample. The results of the frequency sweep along with the corresponding 2nd harmonic ($2f_0$) response at each excitation frequency are plotted in Figure 8.

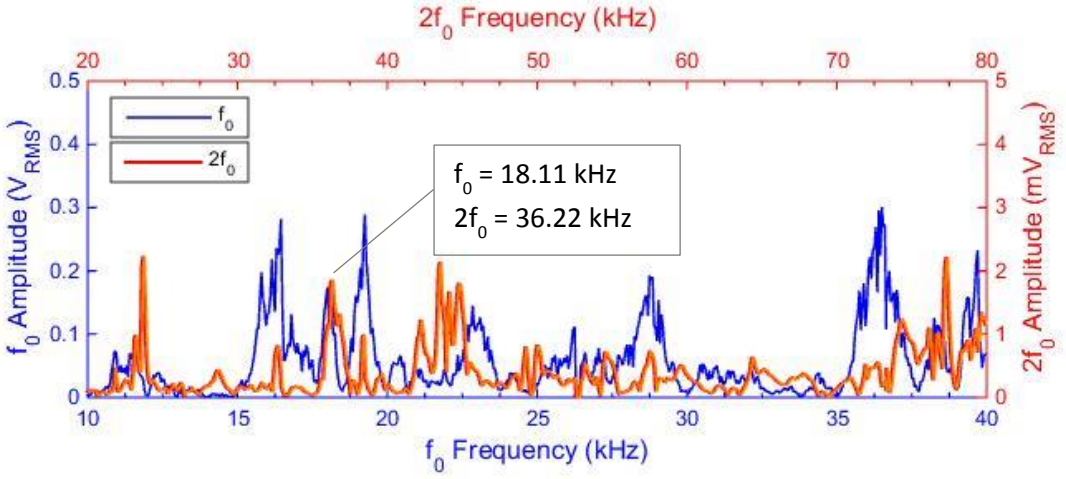

Figure 8: fundamental and 2nd harmonic frequency response of the sample with w_d of 20 mm.

As it can be seen from Figure 8, a clear amplitude peak of the fundamental and its 2nd harmonic frequency was observed at f_0 = 18.11 kHz which is in close spectral proximity to its numerically obtained counterpart (i.e. 18.06 kHz). Experimentally obtained time averaged spectrum from single-frequency excitation is shown in Figure 9(a), whereas the plot of the frequency spectrum of the nodal velocities generated in the numerical analysis is displayed in Figure 9(b). The data presented in Figure 9 was normalised according to the fundamental frequency so that its amplitude starts at 0 dB.

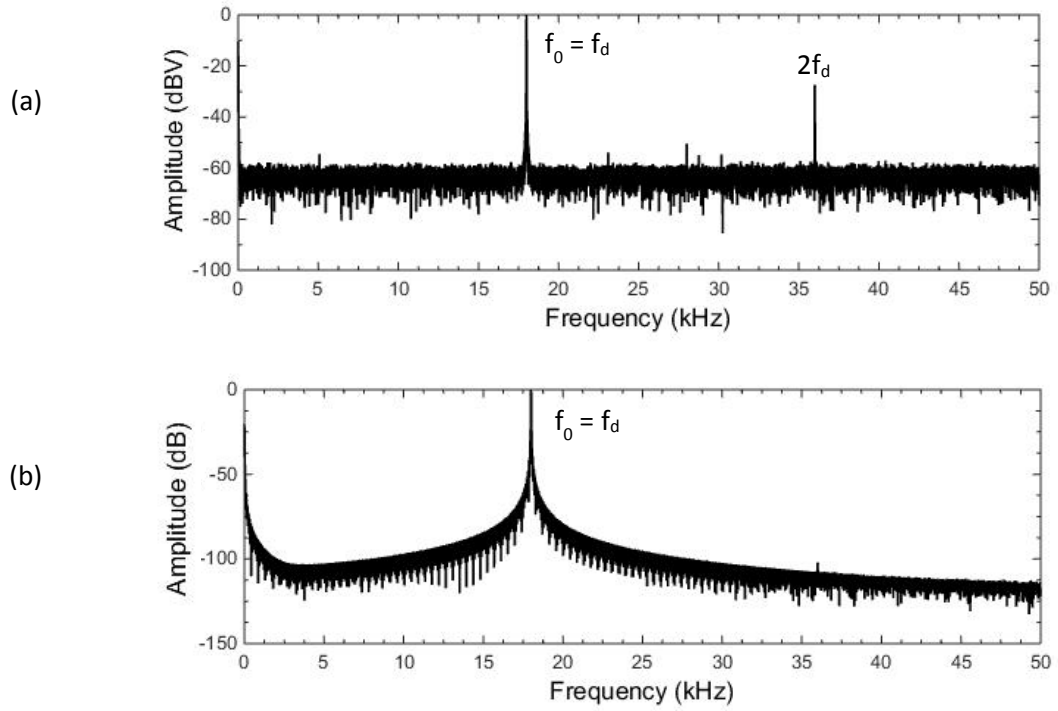

Figure 9: (a) experimental (PZT) and (b) numerical simulation (LS-DYNA) results showing a fundamental-normalised frequency response spectrum obtained using a single-tone excitation.

In order to verify that the experimentally obtained response at 18.11 kHz was indeed associated with the flexural mode, a LDV was used to measure the out-of-plane velocity at the surface of the sample while exciting the sample at f_0 = 18.11 kHz. The plot of the vibration amplitude recorded by the LDV is presented in Figure 10(b).

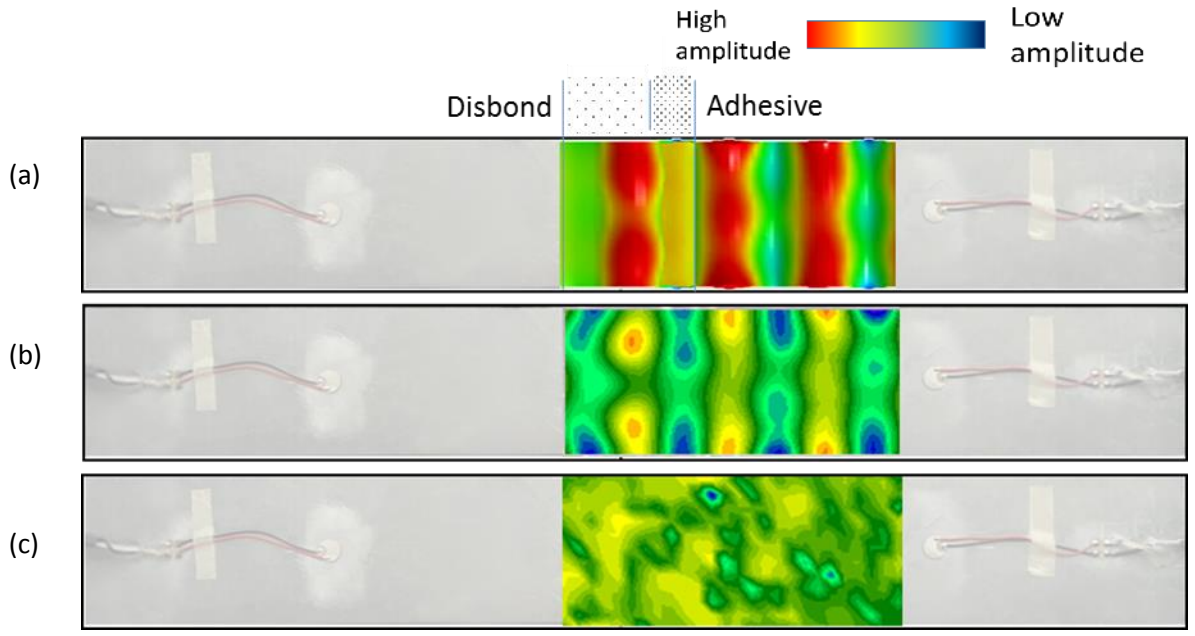

Figure 10: (a) numerically (LS-DYNA) obtained out-of-plane displacement of the sample signifying a flexural mode at 18.06 kHz; (b) experimental (LDV) results – amplitude of the driving vibration velocity at f_0 = 18.11 kHz and (c) the amplitude of the 2nd harmonic ($2f_0$ = 36.22 kHz) spectral component of the vibration velocity as obtained using LDV.

Subsequently, the existence of the flexural mode at f_0 = 18.11 kHz was experimentally confirmed which correlates well with the out-of-plane response obtained numerically via modal analysis (Figure 10(a)). The plot of the 2nd harmonic amplitude (Figure 10(c)) of the frequency spectrum for the corresponding f_0 does not clearly indicate the presence of the disbond, although, a moderate increase in the vibration amplitude can be observed in its vicinity. According to the analytical model, a subharmonic frequency component $f_0 - f_d$ should exit at $f_0 = 2 f_d$ = 36.22 kHz in case 18.11 kHz is in fact f_d corresponding to the LDR frequency associated with the disbond. The existence of this subharmonic component was confirmed by plotting the subharmonic response $0.5 f_0$ for each fundamental frequency of excitation f_0, which was obtained following the first experimental setup involving the two PZT transducers; the outcome is displayed in Figure 11.

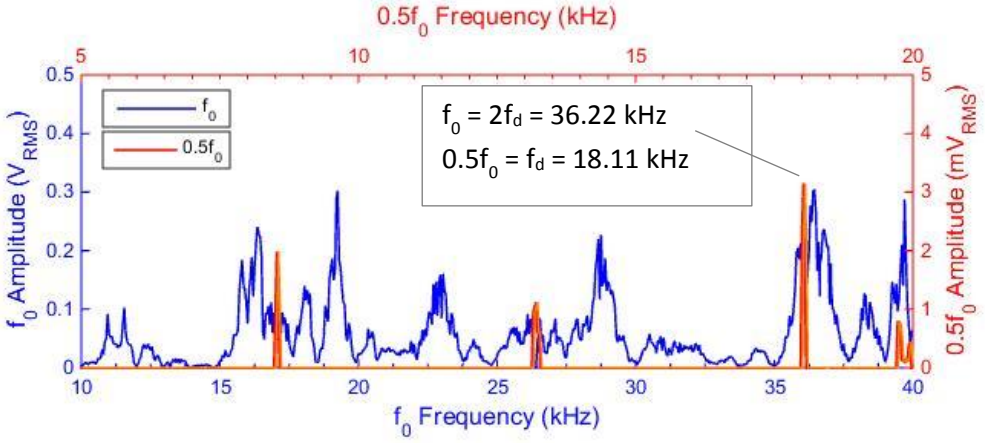

Figure 11: fundamental and subharmonic frequency response of the sample with w_d of 20 mm.

By means of a single frequency excitation ($f_0 = 2f_d$) using the experimental setup reported in the previous section, a time averaged frequency spectrum was achieved both experimentally for the voltage amplitude (Figure 12(a)) and numerically for the frequency spectrum of nodal velocities (Figure 12(b)).

(a)

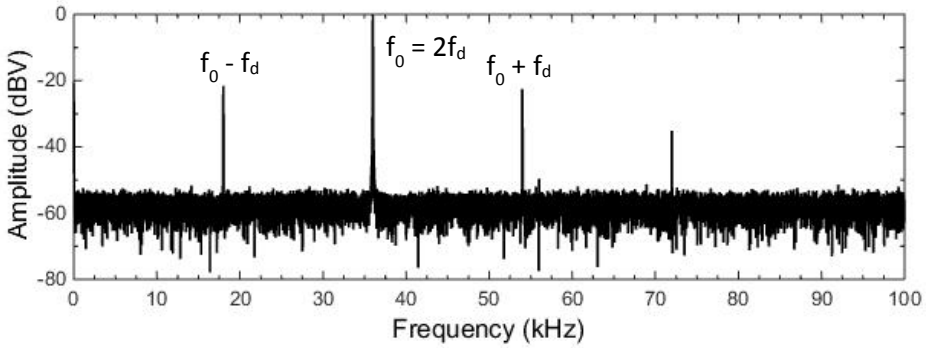

(b)

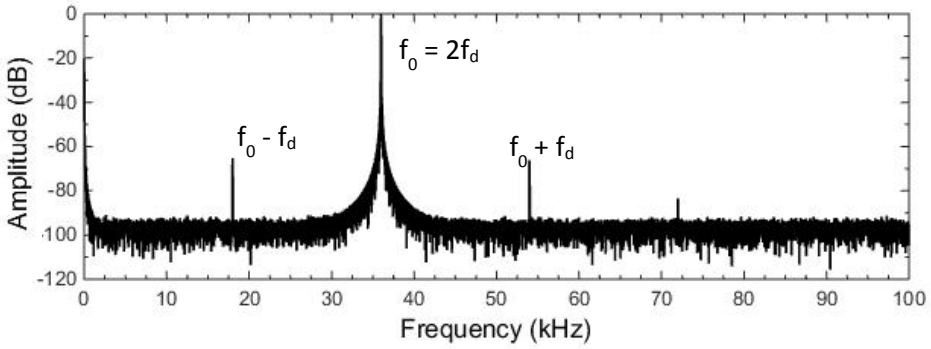

Figure 12: fundamental-normalised frequency response spectrum obtained (a) experimentally (PZT) and via (b) numerical simulation (LS-DYNA).

Evidently, both the experimentally and computationally attained frequency responses of the sample under the excitation frequency of $2f_d$ contained the combination frequencies ($f_0 \pm f_d$) predicted by the analytic model. Furthermore, Figure 11 shows that in comparison to the 2nd harmonic response (Figure 8), there is only a small number of peaks associated with the subharmonic frequencies. This may be explained by the fact that the 2nd harmonic generation is a more frequent and common nonlinear phenomenon occurring at a broad range of frequencies and indeed often produced by the instrumentation itself. In this respect, the subharmonic response can be more advantageous and provided a clear localisation of the debonded region during the subsequent LDV experiments as presented in Figure 13.

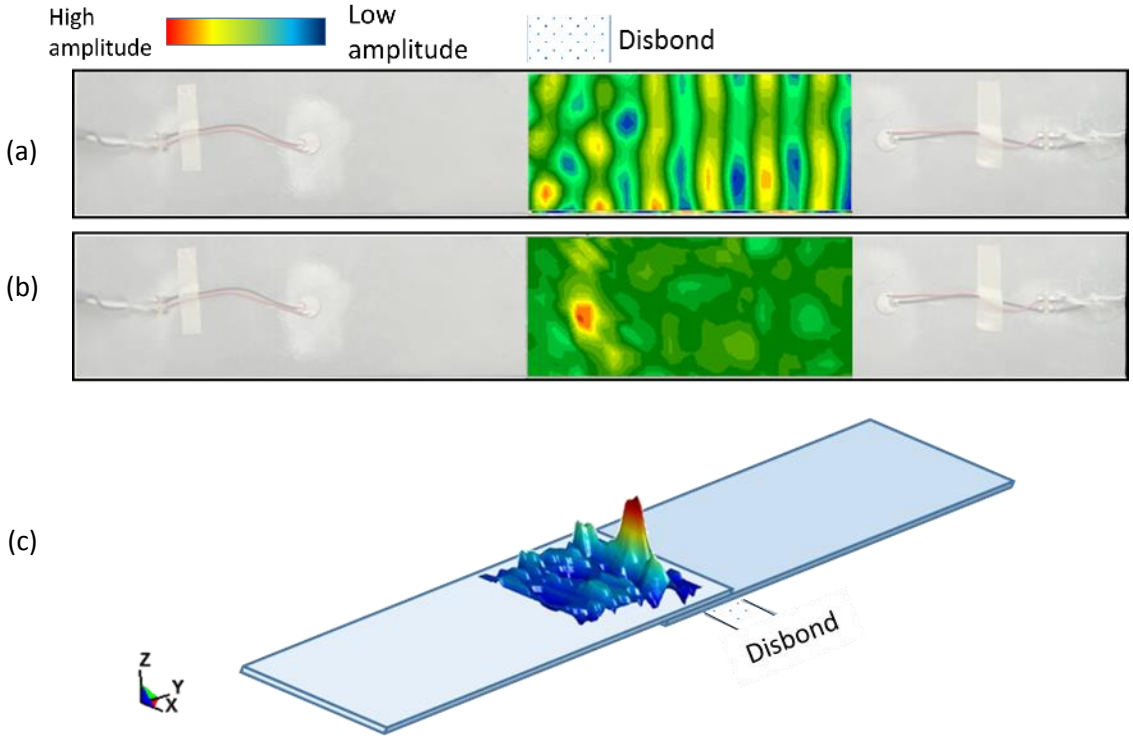

Figure 13: (a) experimental (LDV) results – amplitude of the vibration velocity at $f_0 = 2f_d$ = 36.22 kHz and (b) the amplitude of its spectral component at $0.5f_0$ = 18.11 kHz which is also $f_0 - f_d = f_d$; (c) a 3D surface plot of $0.5f_0$ amplitude obtained via LDV experiments.

Whilst Figure 13 (a) does not show any amplitude peak around the debonded region at the fundamental frequency, Figure 13(b) displays a localised amplitude increase at the subharmonic frequency component as a colour contrast in the vicinity of the disbond. Figure 13(c) further visualises this nonlinear effect by assigning each point depth values according to its colour and displaying the out-of-plane vibrational response with the LDV.

The experimental and numerical procedures involving single frequency excitation were repeated using samples and computational models with various disbond widths (see Table 2). The corresponding amplitude results at f_0 and $0.5f_0$ against the recess width are shown in Figure 14; the data was normalised to the maximum value for each series of results, while the curves represent a polynomial fit for each series of results.

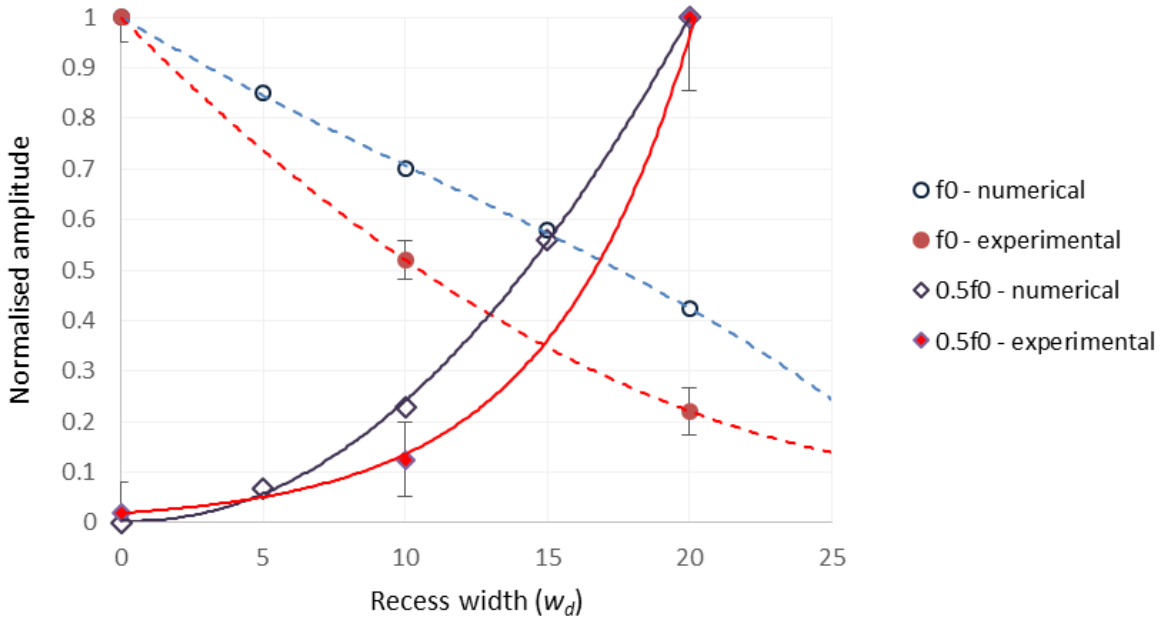

Figure 14: amplitude of the driving and the subharmonic frequency response at the excitation frequency of $2f_d$ normalised to the maximum value for each series of results; error bars represent standard deviation.

As expected, the amplitude of response at the driving frequency reduced with increasing disbond width as less energy propagates into the other aluminium plate of the SLJ sample. On the contrary, the subharmonic amplitude increased with increasing recess width of the debonded region. This further confirms the dependence of the subharmonic generation on the extent of the disbond. Although the input signal amplitude was kept constant in the experimental and numerical studies, the production of subharmonics is known to be strongly dependent on the input amplitude [32] and may need to be adjusted in other testing scenarios. The discrepancies between the numerical and experimental results can be explained by a multitude of factors and assumptions adopted for the computational approach. For example, no damping was used in the developed FEA model as it was not essential for the qualitative nature of the study.

Conclusion

A two dimensional analytical model based on nonlinear oscillator was provided considering a plate in bending. The analytical model qualitatively indicated the generation of higher harmonics and the combination frequencies corresponding to the nonlinear intermodulation of the driving and the defect resonance frequencies. Subsequently, an isotropic single lap joint structure containing a disbond was considered in the experimental and numerical campaign. The LDR associated with the debonded

region was identified via modal analysis, which was experimentally confirmed using surface-bonded piezoelectric transducers and laser-Doppler vibrometer. In line with the existing literature, it was confirmed that an effective subharmonic sensing can be achieved by exciting the sample at twice the value of the flexural (natural) mode of vibration. Subsequently, the nonlinear imaging of the defect using subharmonic spectral component was successfully performed. Furthermore, a numerical model of partially bonded single lap joint was devised using a finite element analysis (FEA) software LS-DYNA® with user defined cohesive elements representing the disbond. The cohesive model incorporating quadratic stiffness relationship in the debonded region successfully predicted the generation of subharmonic frequencies in presence of the defect.

Acknowledgment

Michele Meo would acknowledge EU 7th framework programme “ALAMSA” project (agreement number 314768) and Francesco Ciampa would acknowledge the EPSRC “NUSIT” (EP/N016386/1) project.

References

1. de Lima, W.J.N. and M.F. Hamilton, *Finite-amplitude waves in isotropic elastic plates.* Journal of Sound and Vibration, 2003. **265**(4): p. 819-839.
2. Nayeb-Hashemi, H. and J. Rossettos, *Nondestructive Evaluation of Adhesively Bonded Joints by Acousto-Ultrasonic Technique and Acoustic Emission*, in *Final contract NAG3-1129 Report*. 1997, NASA Lewis Research Center.
3. Zhou, W., et al., *Acoustic emission behaviors and damage mechanisms of adhesively bonded single-lap composite joints with adhesive defects.* Journal of Reinforced Plastics and Composites, 2015. **34**(1): p. 84-92.
4. Khalil, A.A. and A.N. Kagho, *Non-destructive testing of adhesively bonded joints using vibrational analysis.* International Journal of Adhesion and Adhesives, 1991. **11**(2): p. 121-127.
5. Roth, W. and V. Giurgiutiu, *Structural health monitoring of an adhesive disbond through electromechanical impedance spectroscopy.* International Journal of Adhesion and Adhesives, 2017. **73**: p. 109-117.
6. Malinowski, P., T. Wandowski, and W. Ostachowicz, *The use of electromechanical impedance conductance signatures for detection of weak adhesive bonds of carbon fibre–reinforced polymer.* Structural Health Monitoring, 2015. **14**(4): p. 332-344.
7. Nagy, P.B., *Ultrasonic classification of imperfect interfaces.* Journal of Nondestructive Evaluation, 1992. **11**(3-4): p. 127-139.
8. Vine, K., P. Cawley, and A. Kinloch, *The correlation of non-destructive measurements and toughness changes in adhesive joints during environmental attack.* The Journal of Adhesion, 2001. **77**(2): p. 125-161.
9. Yamanaka, K., T. Mihara, and T. Tsuji, *Evaluation of closed cracks by model analysis of subharmonic ultrasound.* Japanese journal of applied physics, 2004. **43**(5S): p. 3082.
10. Amerini, F. and M. Meo, *Structural health monitoring of bolted joints using linear and nonlinear acoustic/ultrasound methods.* Structural Health Monitoring, 2011: p. 1475921710395810.
11. Rothenfusser, M., M. Mayr, and J. Baumann, *Acoustic nonlinearities in adhesive joints.* Ultrasonics, 2000. **38**(1): p. 322-326.
12. Ginzburg, V., *The theory of Luxemburg–Gorky effect.* Izvestiya Akademii Nauk SSR, Seriya Fizicheskaya, 1948. **12**: p. 253.
13. Ciampa, F., et al., *Nonlinear imaging of damage in composite structures using sparse ultrasonic sensor arrays.* Structural Control and Health Monitoring, 2017. **24**(5).
14. Ciampa, F., G. Scarselli, and M. Meo, *Nonlinear imaging method using second order phase symmetry analysis and inverse filtering.* Journal of Nondestructive Evaluation, 2015. **34**(2): p. 1-6.
15. Ciampa, F., et al., *Nonlinear elastic wave tomography for the imaging of corrosion damage.* Ultrasonics, 2015. **62**: p. 147-155.
16. Solodov, I. *Nonlinear Acoustic NDT: Approaches, Methods, and Applications*. in *Proceedings NDT in Progress, 5th International Workshop of NDT Experts. Prague*. 2009.
17. Solodov, I., et al., *Nonlinear self-modulation and subharmonic acoustic spectroscopyfor damage detection and location.* Applied physics letters, 2004. **84**(26): p. 5386-5388.
18. Sarens, B., et al., *Investigation of contact acoustic nonlinearity in delaminations by shearographic imaging, laser doppler vibrometric scanning and finite difference modeling.* Ultrasonics, Ferroelectrics, and Frequency Control, IEEE Transactions on, 2010. **57**(6): p. 1383-1395.
19. Pecorary, C. and I. Solodov, *Non-classical nonlinear dynamics of solid interfaces in partial contact for NDE applications.* Universality of Non-Classical Nonlinearity with Application to NDE and Ultrasonics, 2006. **19**: p. 307-324.
20. Landau, L. and E. Lifshitz, *Classical mechanics*. 1960, Pergamon Press, Oxford.
21. Hirsekorn, S. and P.P. Delsanto, *On the universality of nonclassical nonlinear phenomena and their classification.* Applied physics letters, 2004. **84**(8): p. 1413-1415.

22. Solodov, I., *Resonant Acoustic Nonlinearity of Defects for Highly-Efficient Nonlinear NDE.* Journal of Nondestructive Evaluation, 2014. **33**(2): p. 252-262.
23. Solodov, I., J. Bai, and G. Busse, *Resonant ultrasound spectroscopy of defects: case study of flat-bottomed holes.* Journal of Applied Physics, 2013. **113**(22): p. 223512.
24. De Angelis, G., et al., *A new technique to detect defect size and depth in composite structures using digital shearography and unconstrained optimization.* NDT & E International, 2012. **45**(1): p. 91-96.
25. Meo, M., U. Polimeno, and G. Zumpano, *Detecting damage in composite material using nonlinear elastic wave spectroscopy methods.* Applied composite materials, 2008. **15**(3): p. 115-126.
26. Wang, Z., W. Qu, and L. Xiao. *Nonlinear Ultrasonic Damage Detection for Fatigue Crack Using Subharmonic Component*. in *EWSHM-7th European Workshop on Structural Health Monitoring*. 2014.
27. Solodov, I., et al., *Nonlinear self-modulation and subharmonic acoustic spectroscopy for damage detection and location.* Applied Physics Letters, 2004. **84**(26): p. 5386-5388.
28. Delrue, S. and K. Van Den Abeele, *Three-dimensional finite element simulation of closed delaminations in composite materials.* Ultrasonics, 2012. **52**(2): p. 315-324.
29. Yamanaka, K., et al., *Two-Dimensional Analyses of Subharmonic Generation at Closed Cracks in Nonlinear Ultrasonics.* Applied physics express, 2011. **4**(7): p. 076601.
30. Kneubühl, F.K., *Oscillations and waves*. 2013: Springer Science & Business Media.
31. Ciampa, F., G. Scarselli, and M. Meo, *On the generation of nonlinear damage resonance intermodulation for elastic wave spectroscopy.* The Journal of the Acoustical Society of America, 2017. **141**(4): p. 2364-2374.
32. Ohara, Y., T. Mihara, and K. Yamanaka, *Effect of adhesion force between crack planes on subharmonic and DC responses in nonlinear ultrasound.* Ultrasonics, 2006. **44**(2): p. 194-199.
33. Jhang, K.-Y., *Nonlinear ultrasonic techniques for nondestructive assessment of micro damage in material: a review.* International journal of precision engineering and manufacturing, 2009. **10**(1): p. 123-135.
34. Kim, G.-W., et al., *Localization of breathing cracks using combination tone nonlinear response.* Smart Materials and Structures, 2011. **20**(5): p. 055014.
35. Naito, K. and T. Sugiura. *A possible mechanism causing subharmonics in ultrasonic testing of a closed crack*. in *Ultrasonics Symposium (IUS), 2010 IEEE*. 2010. IEEE.
36. Hearn, G. and R.B. Testa, *Modal analysis for damage detection in structures.* Journal of Structural Engineering, 1991. **117**(10): p. 3042-3063.
37. Ewins, D.J., *Modal testing: theory and practice*. Vol. 15. 1984: Research studies press Letchworth.